Korean J. Chem. Eng., 36(9), 1518-1526 (2019)
DOI: 10.1007/s11814-019-0344-5

pISSN: 0256-1115
eISSN: 1975-7220

Synthesis of InP nanocrystals using triphenyl phosphite as phosphorus source

Dongkyu Lee*, Sungjun Koh*, Da-Eun Yoon*, Sooho Lee*, Whi Dong Kim*, Dahin Kim*, Wan Ki Bae, Jaehoon Lim***, and Doh C. Lee*,†**

*Department of Chemical and Biomolecular Engineering (BK21+ Program), KAIST Institute for the Nanocentury, Korea Advanced Institute of Science and Technology (KAIST), Daejeon 34141, Korea
**SKKU Advanced Institute of Nano Technology, Sungkyunkwan University, Gyeonggi 16419, Korea
***Department of Chemical Engineering and Department of Energy System Research, Ajou University, Suwon 16499, Korea
(*Received 3 March 2019 • accepted 19 July 2019*)

Abstract−Commercially viable synthesis of InP nanocrystals (NCs) involves highly pyrophoric phosphorus (P) precursor, tris(trimethylsilyl) phosphine (TMS_3P). Finding a cheap and safe alternative would be the holy grail. We report the synthesis of InP NCs using triphenyl phosphite, an inexpensive and relatively safe phosphorous source. By reacting indium chloride and triphenyl phosphite, we obtained large-sized and black-colored InP NCs, yet without any distinct feature that shows quantum confinement effect. Addition of $ZnCl_2$ resulted in InP NCs with controlled size, which was manifested in the shift of 1S peak in absorption spectra. By coating ZnS shell on InP NCs, we achieved photoluminescence with some extent of trap emission, showing maximum total quantum yield (QY) of 23% (8% of band-edge emission QY). We used ^{31}P nuclear magnetic resonance (NMR), diffusion-ordered spectroscopy (DOSY), and mass spectrometry (MS) to assign intermediates and following mechanisms of the InP synthesis using triphenyl phosphite. The development of this safe and cost-effective P precursor opens broader opportunity space for large-scale production of InP NC.

Keywords: InP Nanocrystals, Triphenyl Phosphite, Phosphorus Precursor

INTRODUCTION

Semiconductor nanocrystals (NCs) have attracted great interest for their fundamentals and applications because of their unique size-dependent properties [1-5]. The past two decades have witnessed intense progress in research, from designing their surface [6-8], shape [9,10] and unique structures [11-16] to their in-depth physical [17-19] and chemical properties [20,21]. Among these, indium phosphide (InP) NCs as next-generation material for light emitting diodes (LEDs) have motivated intense studies on their properties, synthesis and its engineering [22-28]. One of the biggest issues in designing InP NCs stems from the scarcity of good phosphorus (P) precursors, which show their own limitations on their cost, safety, or reactivity during synthetic procedure. These limitations have attracted a huge interest in developing new P precursors to obtain a large amount of high quality InP NCs with lowest cost using safest synthetic procedure.

Various types of P precursors have been reported, such as trioctylphosphine (TOP) [29], Ca_3P_2 [30], TOP-P_4 [31], aminophosphines [32,33], and most widely, tris(trimethylsilyl) phosphine ($(TMS)_3P$) [24]. These P precursors, in particular $(TMS)_3P$, are mostly hazardous and expensive chemicals which cause severe potential threat during conventional synthetic process. Therefore, the research on activating safer and cheaper P precursors such as aminophosphines have been performed to address these issues of $(TMS)_3P$. The studies on aminophosphines are concerned as significant improvement because aminophosphines are easier to handle and cheaper than $(TMS)_3P$.

All these P precursors, in particular $(TMS)_3P$, are mostly hazardous and expensive chemicals, which cause severe potential threat during conventional synthetic process. Therefore, research on activating safer and cheaper P precursors, such as aminophosphines, have been performed to address these issues of $(TMS)_3P$. The studies on aminophosphines are concerned as significant improvement because aminophosphines are easier to handle and cheaper than $(TMS)_3P$.

In this context, trialkyl phosphites are promising alternative of P source because they are typically not flammable and not explosive with low price which is less than one thousandth of $(TMS)_3P$ [34, 35]. In addition, it is known that phosphites participate in Arbuzov reaction with transition metal halides to produce metal-phosphite complex [36,37]. If indium-phosphite composites are formed, these complexes might be reformed into In-P monomers possibly resulting in InP QDs.

Among various phosphites, triphenyl phosphite (TPP) would be the most effective P precursor for InP synthesis, since three benzene rings would stabilize the partial charges for In-P monomer formation. In fact, TPP is reported as an effective phosphine source for the synthesis of various metal phosphide nanocrystals such as Ni_2P or Co_2P, although trials on producing InP NCs have failed [34]. The failure may stem from the difficulty of matching the right combination of precursors and ligands that can activate P source to form In-P monomers.

The mechanisms of some P precursor activation and following

†To whom correspondence should be addressed.
E-mail: dclee@kaist.edu

monomer formation have been reported in a few articles. In the publications regarding $(TMS)_3P$, $(TMS)_3P$ directly forms a complex with indium halide. Then, the complex becomes In-P monomer after successive methylsilyl group dissociation. In-P monomer formation often requires structural change of P precursor to be activated. This is, for example the case for TOP and aminophosphines. Reports on TOP activation note that TOP suffer P-C bond dissociation under presence of indium metal, then react with In(0) powder to form In-P monomers [38]. The activation of aminophosphines is known to include $P(oleylamine(OLA))_3$ intermediate formation followed by acid-base and redox reaction to form three P(5+) species and one In-P(-3) intermediate [33].

Throughout the mechanism, the key to P precursor activation and In-P monomer formation is to reduce central phosphorus atom within P precursors. When a phosphorus atom in P precursor has +3 charges, repulsive columbic interaction between P^{3+} and In^{3+} hinders In-P monomer formation. From this perspective, $(TMS)_3P$ or even $(TMGe)_3P$ [39] can be used without phosphorus reduction since less electronegative Si and Ge allow central P atom to have negative charge. Because of this natural negative charge of the P atom, $(TMS)_3P$ have been considered as representative P source in InP synthesis. The known mechanisms of other precursors follow the similar logic. In the case of aminophosphines, OLA transforms aminophosphines into a suitable form to be further reduced via internal redox reaction. The mechanisms regarding TOP, Ca_3P_2, and TOP-P_4 are not yet thoroughly clear; however, authors note that central P should be reduced at least to neutral P(0) or more negative form [29-33]. Therefore, development of new P precursor includes not only the exploration of validating In-P precursor combination, but also the reduction and activation of central P atom within P precursors.

Here, we report TPP activation and its consequent novel InP NCs synthesis. A series of trial-and-error processes based on the fundamentals of phosphorus reduction and activation was our key strategy of developing the novel InP synthesis using TPP. Control of temperature, reaction time, and the amount of adding $ZnCl_2$ enable the size tuning of resultant InP NCs within quantum confinement regime. In addition, we provide a possible mechanism of TPP activation and In-P monomer formation via nuclear magnetic resonance (NMR), mass spectrometry and diffusion ordered spectroscopy (DOSY).

RESULTS AND DISCUSSION

The research on TPP activation in InP NCs synthesis originated from a patent, providing InP NCs synthetic recipe using triethyl phosphite or TPP with indium oleate in 1-octadecene (ODE) [40]. As described in the introduction part, the activation of TPP requires the central P reduction followed by P-O bond cleavage. Therefore, the right choice of In-P precursor pair is necessary for successful InP NCs synthesis.

Fig. 1 provides a set of UV-VIS spectra and X-ray diffraction (XRD) patterns of InP NCs synthesized with $InCl_3$-OLA complex and indium carboxylates, respectively. To activate TPP by reduction of the central P atom, we introduced $InCl_3$-OLA complex as In precursor. In the previous research, aminophosphines could be acti-

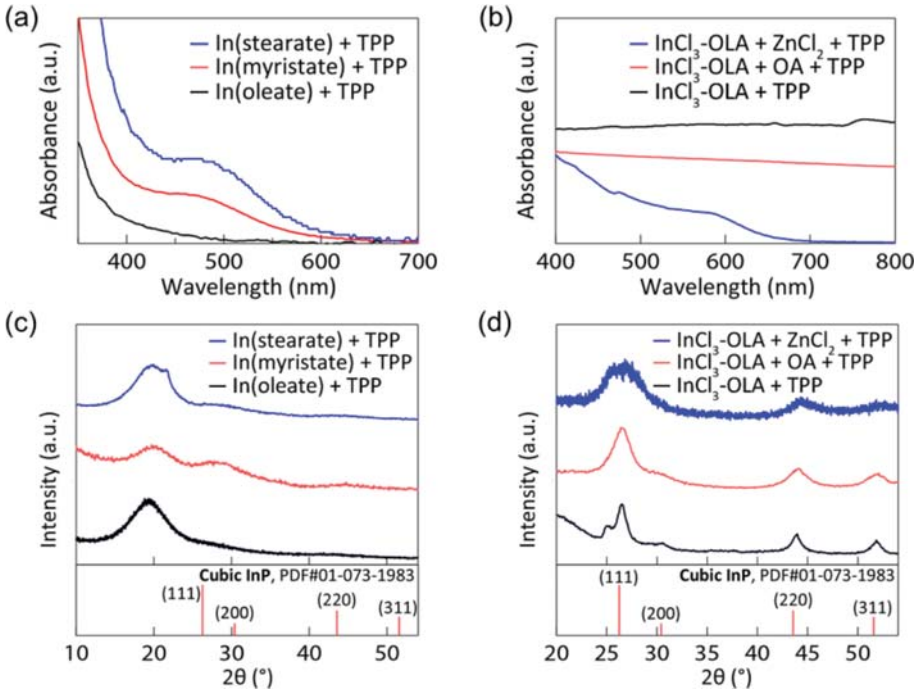

Fig. 1. UV-VIS spectra and XRD patterns of InP nanocrystals which were synthesized with (a), (c) indium carboxylates in 1-octadecene (ODE) at 300 °C for 1 hour and (b), (d) $InCl_3$-OLA complex in trioctylamine (TOA) and OLA using TPP. In Fig. (b) and (d), '$InCl_3$-OLA' and 'oleic acid (OA) added' sample were prepared at 300 °C for 1 hour. In 'OA added' sample, 0.2 mmol of OA was additionally injected before precursor injection as growth-rate controller. '$ZnCl_2$ added' sample was prepared at 220 °C for 10 min. 1 mmol of $ZnCl_2$ (5 *equiv.* moles of indium) was used as a growth-rate controller.

vated by OLA to form $P(NHR)_3$ (R: oleyl group) species as intermediate, followed by internal redox reactions to form In(3-) species [33]. Since amine acts as Lewis basic ligand, TPP would be reduced by these amines to form In-P monomer. The black lines of Fig. 1(b) and 1(d) represent the UV-VIS spectra and XRD pattern of InP NCs synthesized with $InCl_3$-OLA complex. When $InCl_3$-OLA was used with TOA as solvent, black powder appeared after the purification process. The powder could not be dispersed in organic solvents. The black color is characteristic of bulk InP, indicating that large InP crystals were formed. The UV-VIS spectrum did not show any characteristic peak, mainly because of severe aggregation of the powder. XRD analysis followed by using Scherrer equation reveals that 13.8 nm-sized cubic-InP NCs were formed with few unknown byproducts. Since the Bohr radius of InP is known as ~15 nm [41], the produced NCs are nearly in bulk regime, which is barely useful in display application.

However, all the synthetic trials using carboxylic acids instead of amines failed to form InP NCs. When indium oleate was used as In precursor, 1S absorption peak could not be identified, as shown in Fig. 1(a). When other types of indium carboxylates (e.g., indium myristate or stearate) were used, 1S absorption peak appeared at ~480 nm and ~490 nm for indium myristate and stearate product, respectively. However, XRD analysis (Fig. 1(c)) indicates that the resultant InP NCs lack crystallinity, which can be identified by a broad peak at ~20° 2-theta degree. Moreover, absent or weak major diffractions from *cubic*-InP lattice indicate that the produced NCs are mostly in amorphous phase. The production of amorphous particles represents incomplete reduction of TPP. Since carboxylates are Lewis acidic ligands, the central P atom within TPP could not be reduced from P(3+) to negative charged state. This may hinder the In-P monomer formation and crystallization due to In^{3+} by Coulombic repulsion, resulting amorphous InP formation.

To control the growth kinetics of NCs to reduce their size into quantum confinement regime, we tried the addition of OA as a potential growth rate controller [42,43]. The idea stems from the known fact that OA and oleate ions affect NC growth by forming lamellar micelles, which stabilize NCs. When 0.2 mmol of OA was added along with $InCl_3$-OLA, XRD analysis and Scherrer equation indicate the formation of 6.4 nm-sized perfect InP NCs, while no distinct absorption peak was observed (Fig. 1(b)). Adding more than 0.3 mmol of OA led to no color change during the reaction and no precipitates after purification, indicating the failure of InP NCs production. The failure can be understood in a similar way with the amorphous InP formation that Lewis acidic OA hinders the TPP activation by amines. The dilemma between smaller NCs size and TPP activation by reduction implies that other rate controlling material is required.

The other known method to control InP NCs growth is to add zinc source into the InP synthetic protocol. It was previously reported that additional zinc source forms stable Zn-P intermediate complex which can slow down the NCs growth kinetics [28]. Because TPP activation suffers similar In-P monomer formation process before crystal growth, the introduction of Zn source to form stable Zn-P intermediate would also be effective in relieving InP growth kinetics in the case of TPP. Indeed, UV-VIS spectrum and XRD pattern of the resultant NCs (The blue lines in Fig. 1(b) and 1(d)) indicate the formation of the perfect crystalline InP NCs. The XRD pattern clearly follows the typical pattern of cubic-InP crystal but slightly shifted to higher degree. The shift is due to the formation of ZnP lattice within InP NCs, which indicates that the resultant NCs would be InZnP NCs. The size measurement using Scherrer equation revealed the size of the InZnP NCs is 4.5 nm. This is well-matched with the UV-VIS spectrum showing 1S peak at ~590 nm, which was calculated as 4.3 nm-sized InP NCs. Photoluminescence (PL) signal of the NCs did not appear, which may due to severe surface defects.

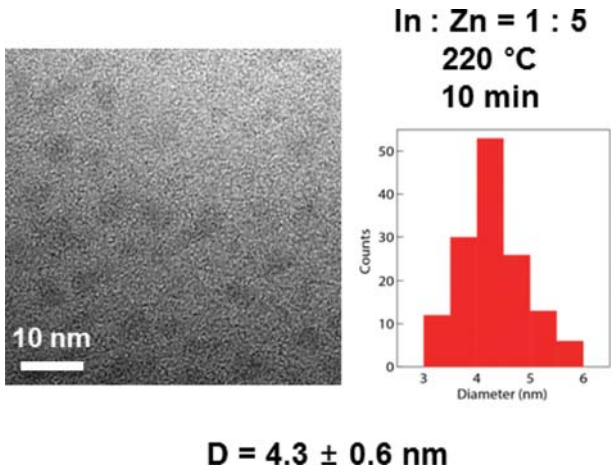

Fig. 2. TEM images of InZnP NCs synthesized with 5 molar equiv. Zn source to In at 220 °C for 10 min. The histogram implies that the size of produced NCs is 4.3±0.6 nm.

Fig. 2 shows representative TEM image of produced InZnP NCs. The image clearly shows the formation of spherical-shaped InZnP NCs with the size of 4.3±0.6 nm. The measured size is again well-matched with the size derived from UV-VIS spectra and XRD patterns, which implies that Zn addition is definitely effective in NC growth suppression.

To inspect the effect of additional Zn source in advance, we performed the synthesis with different Zn/In ratio at different reaction temperature. Fig. 3 summarizes absorption spectra and their 1S peak positions of InZnP NCs produced at various reaction conditions. In general, the addition of zinc source results in the InZnP NCs, which 1S absorption peak is in the visible range. By varying the reaction conditions and Zn/In ratio, the 1S absorption peaks can be controlled from ~450 nm to ~650 nm in wavelength, which covers most of the visible range spectrum. When Zn/In ratio and temperature are too low (*e.g.,* Zn/In=1 at 220 °C or Zn/In=0.5 at 250 °C in Fig. 3), no sign of InP formation appears. The 1S peaks show red-shift when the reaction proceeds, implying that the typical nucleation and growth process also takes place in this InP synthesis using TPP. With the fixed Zn/In ratio, the InZnP NCs grew faster when the higher reaction temperature was applied, indicating that the TPP activation process suffers endothermic process, which is similar to the case of other NCs colloidal growth process. Since TPP activation would include P-O bond cleavage and reduction, the observed endothermic dependence on reaction temperature is considered as a natural phenomenon.

With the fixed reaction temperature, however, increasing Zn/In

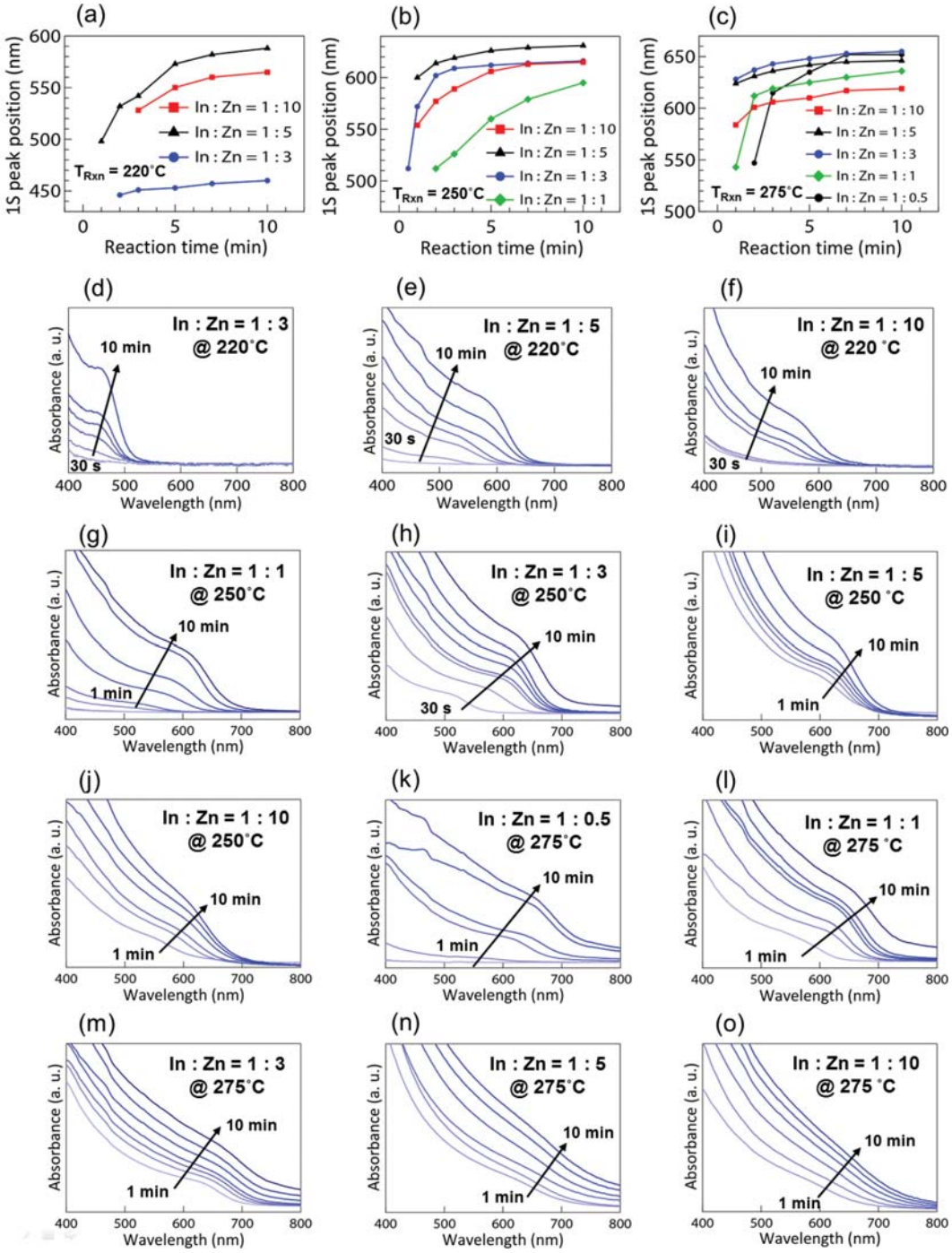

Fig. 3. A summary of 1S peak positions from absorption spectra of InZnP NCs using different Zn/In ratio with various reaction temperatures of 220 °C (a), 250 °C (b) and 275 °C (c), followed by absorption spectra of InZnP NCs using different reaction temperatures of 220 °C (d)-(f), 250 °C (g)-(j) and 275 °C (k)-(o) with various In/Zn ratio. The evolution 1S peaks supports that the growth of InZnP NC takes place as the reaction proceeds.

ratio resulted in faster NCs growth, which is in contradiction with the fact that Zn source greatly suppressed the NCs growth. However, the growth kinetics were suppressed with excess amount of zinc (more than Zn/In ratio=5). This contradiction indicates that zinc source has at least two opposite roles in this specific InP growth: one to accelerate and the other to suppress the NCs growth.

Promoted growth of NCs by Zn can be understood by similar logic of the recent work by Laufersky et al., which reveals the role of Zn in aminophosphine redox process [44]. According to the article, $ZnCl_2$ causes the formation of the activated Zn-N-P complex, which suffers rapid and thermodynamically favorable redox reaction. Further DFT calculation revealed that the electron-withdrawing $ZnCl_2$ catalyzed a series of disproportionation and ligand exchange reaction, which results in the rapid formation of reduced

Table 1. Summary of ICP-MS analysis on InZnP NCs, synthesized at 220 °C for 10 min

Zn/In ratio	In contents (mol %)	Zn contents (mol%)	P contents (mol%)
3	62.1	11.9	26.0
5	57.6	16.0	26.4
10	52.4	18.6	29.0

In-P monomers. Zn would be also effective in TPP activation, since TPP activation requires similar P-O covalent bond cleavage, as P-N bond in aminophosphines. The suppression of NCs growth into visible regime can also be explained by this rapid formation of In-P monomers with the presence of Zn. The rapid formation of In-P monomers by Zn would result in an increased number of InP seeds in the growth process, and therefore smaller sized InP NCs could be obtained. Without Zn, low monomer concentration causes severe Ostwald ripening, which results in large black-colored InP NCs. In addition, the suppression of NCs growth with excess Zn addition (*e.g.*, Zn/In=10) can be understood in a similar way with the case of $(TMS)_3P$, by which excess Zn source additionally forms stable Zn-P complexes, hindering the NCs growth kinetics similar to the synthesis with $(TMS)_3P$ [28].

Table 1 shows ICP-MS analysis results on InZnP NCs synthesized at 220 °C for 10 min using various In/Zn ratio, which further supports the formation of InZnP NCs. For all InZnP NCs, an excess amount of cations within the InZnP NCs was observed. The excess amount of cations is connected with the formation of anion vacancies, which is the source of non-radiative recombination site in III-V semiconductors [45,46]. The formation of non-radiative recombination center results in the absence of PL, and therefore needs to be addressed. This inequality between cations and anions may due to lower reactivity of TPP compared to highly reactive P source such as $(TMS)_3P$. Since this inequality was observed even when the excess amount of TPP (more than 4 *molar equiv.* of In source) was used, other modifications would be necessary to enhance the PL properties.

The most famous method to enhance the optical properties of InP NCs is to grow additional shell layers of ZnS [22,31,47-51]. Growth of ZnS shell on InP core attracted much attention since InP core alone is highly unstable under ambient air and barely photoluminescent without post-treatment. The weak luminescence of InP NCs is due to the existence of non-radiative relaxation channels which originate from surface states. However, the overcoating with a ZnS shell can address these issues to enhance PL of the resultant InP/ZnS core/shell NCs.

Fig. 4 shows UV-VIS and PL spectra of InZnP/ZnS NCs with various known methods of ZnS overcoating. After the introduction of ZnS shell, all the NCs showed PL signals, indicating the partial removal of surface states by ZnS overcoating. However, PL spectra still include luminescence from both red-region (650-700 nm) and near-IR region (>800 nm), implying the presence of emission from trap states. The trap emission was minimized by in-situ ZnS overcoating with zinc acetate, showing 23% of total QY and 8% of band-edge emission QY. While the growth of ZnS shell would relieve surface defects and enhance thermal/chemical stability of

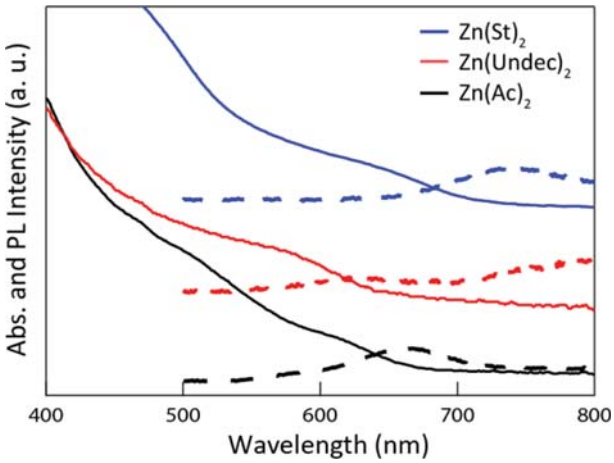

Fig. 4. UV-VIS (solid lines) and PL spectra (dashed lines) of InZnP/ZnS NCs using zinc acetate (black line), zinc undecylenate (red line), and zinc zinc stearate (blue line) as a zinc precursor for ZnS overcoating. InZnP core was synthesized with 5 molar equiv. of Zn at 220 °C for 3 min. ZnS overcoating with zinc acetate showed the best PL property of total 23% of QY and 8% of band-edge emission QY.

NCs, the shelling process cannot recover the internal defects on InP cores, leading to incomplete removal of trap emissions [52,53]. These trap emissions may further be removed by optimization of InP core growth kinetics and overcoating process, or surface etching by fluoride ions. We leave this issue as future work.

UV-VIS, PL, TEM and XRD analyses strongly support the InP NCs synthesis using TPP as P precursor. Then, a natural question arises about how TPP activation and In-P monomer formation occur. We assumed four possible mechanisms for the TPP activation process: (1) the formation of In-phosphite complex by Arbuzov reaction based reaction, (2) direct In-P monomer formation through elemental P formation, (3) TPP activation by substitution of phenyl groups of TPP with oleylamines into $P(OPh)_x(NHR)_{3-x}$ species, (Ph refers benzene ring) and (4) reduction of TPP by OLA via formation of P-N partial bond and consequent P-N intermediate species.

As mentioned in the introduction, phosphites can produce metal-phosphite complex in the presence of amines and metal chlorides [36,37]. If $In[P(OPh)_3]_x$ complex is observed by NMR measurement, it is supported that the In-P monomer formation may be dominated by these In-phosphite complex formation. To identify the validity of the assumption, we performed ^{31}P NMR analysis on the mixtures of indium chloride, amines and TPP (Fig. 5(a)). Simulation from MestReNova program presents that the signal from In-phosphite complex appears at around −250 ppm, originating from the P atom bonded to indium metal and three oxygen atoms. However, All the NMR spectra did not show any signal at −250 ppm, implying that the TPP activation is not promoted by Arbuzov reaction.

Recent study implies that TOP-P_4 acts as an effective P precursor for InP synthesis. In this study, the NMR analysis indicated the direct usage of elemental P_4 by indium metal ions to form In-P monomer [31]. Other study also proposed a mechanism of TOP

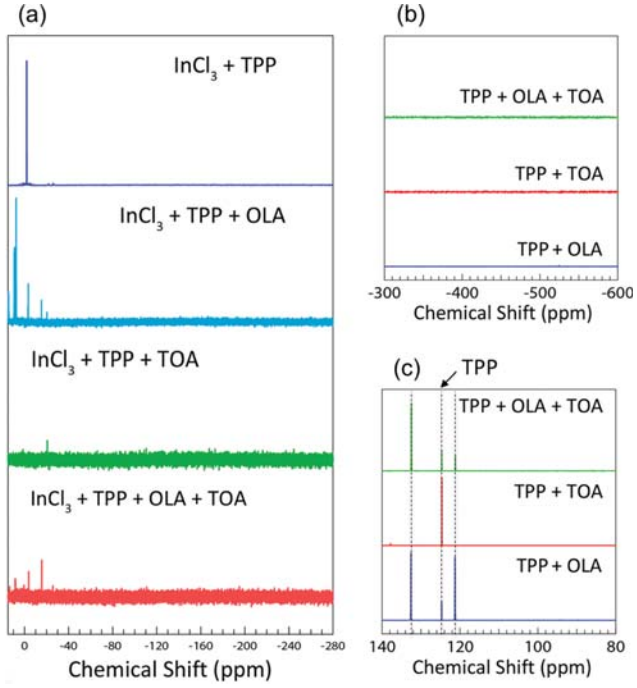

Fig. 5. (a) ^{31}P NMR spectra obtained from the prepared samples of amines-TPP-$InCl_3$ mixtures and ^{31}P NMR spectra of (b) minus chemical shift region and (c) plus chemical shift region, obtained from amines-TPP-only mixtures. Detailed experimental condition is described in experimental section.

activation in InP synthesis that P-C bond are cleaved by external force and resultant P(0) reacts with In(0) to form InP NCs [38]. Therefore, In-P monomer formation via elemental P formation would also be the case of TPP activation. To identify the expected mechanism of elemental P formation, phosphite-amine mixtures were measured by ^{31}P NMR spectra to observe the peak from elemental P at around –520 ppm (Fig. 5(b)). However, the NMR spectra did not show any representative signal of elemental P, implying that TPP activation did not suffer elemental P formation.

Another possible mechanism is substitution of phenyl groups of TPP with OLA into $P(OPh)_x(NHR)_{3-x}$ species, similar to the case of aminophosphines [32,33]. According to the simulation from MestReNova, these $P(OPh)_x(NHR)_{3-x}$ species are expected to be identified at between 100 ppm to 140 ppm. In particular, the signal of $P(NHR)_3$ is known to appear at 98 ppm in the previous report [33]. The signals from the mixtures containing OLA present two major signals of 132.5 and 121.2 ppm, which might be assigned as $P(OPh)_2(NHR)$ and $P(OPh)(NHR)_2$, respectively. (Fig. 5(c)) However, the absence of known signals of $P(NHR)_3$ at ~98 ppm enables one to exclude the possibility of amine substitution and following similar redox reaction as in aminophosphine case. Therefore, the two intermediates at 132.5 and 121.2 ppm would be other chemicals which should be clarified by other measurements. Note that the mixture of TPP and TOA did not produce any intermediates, implying that TOA do not directly participate in TPP reduction, but only act as co-solvent to aid OLA to coordinate indium chloride and to activate TPP. In addition, since OLA and TOA themselves did not show any signals in ^{31}P NMR measurement, these

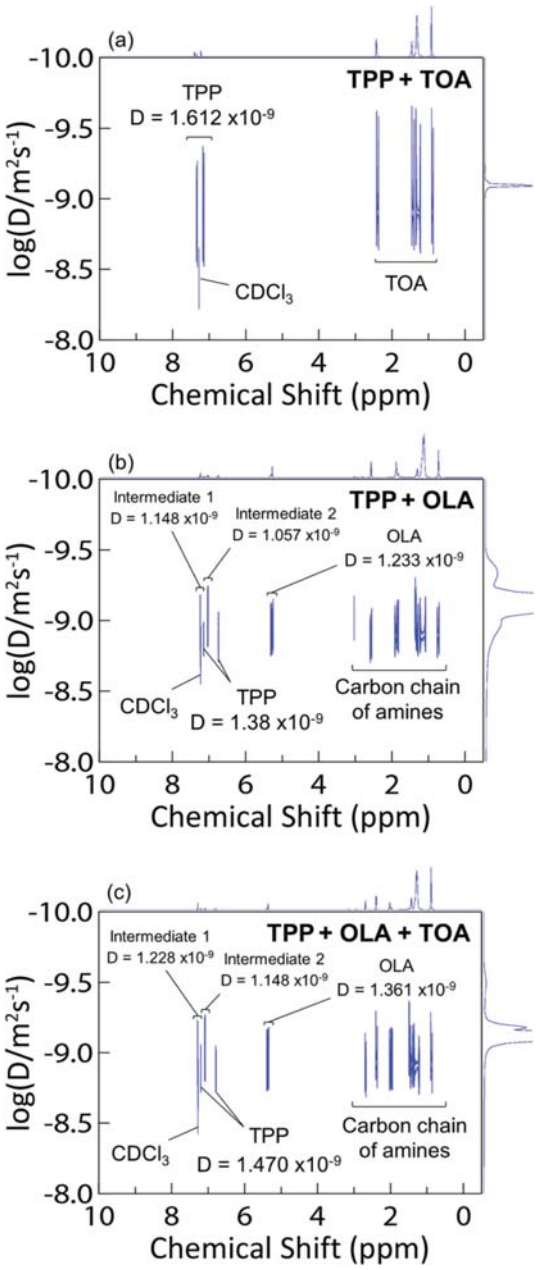

Fig. 6. DOSY spectra for the mixture of (a) TPP in TOA, (b) TPP in OLA, and (c) TPP in OLA and TOA.

two signals are not related with impurities from OLA and TOA.

The set of ^{31}P NMR spectra have excluded the possibility of the three proposed mechanisms and showed the presence of two possible intermediate species. To assign these intermediate species, we performed diffusion ordered spectroscopy (DOSY) for amine-phosphite mixture (Fig. 6). Again, the mixture of TOA and TPP did not show any sign of intermediates (Fig. 6(a)), implying that only OLA has a major role in TPP activation. In contrast, both the samples including OLA (Fig. 6(b) and 6(c)) showed two intermediates with lower diffusivity, compared to TPP. This implies the formation of some other bulkier intermediates and therefore provides another possible mechanism of TPP activation by OLA via formation of P-

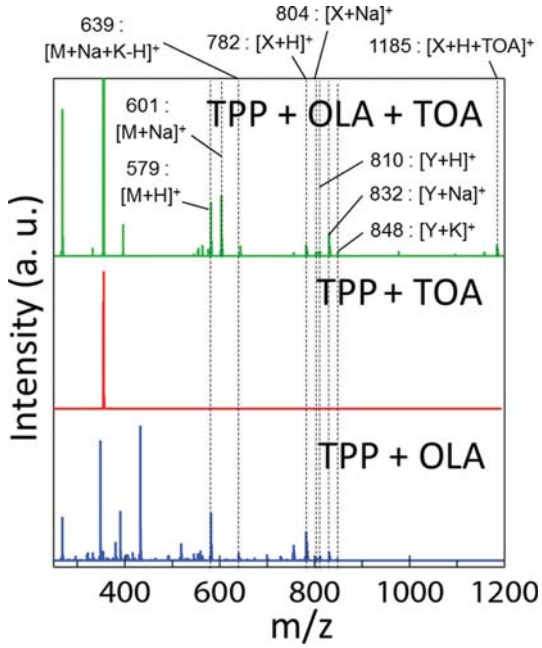

Fig. 7. MS spectra by ESI obtained from the mixtures of TPP in OLA (blue line), TPP in TOA (red line), and TPP in OLA and TOA (green line). Chemical M (578 m/z), X (781 m/z), and Y (809 m/z) could be assigned as possible intermediate species.

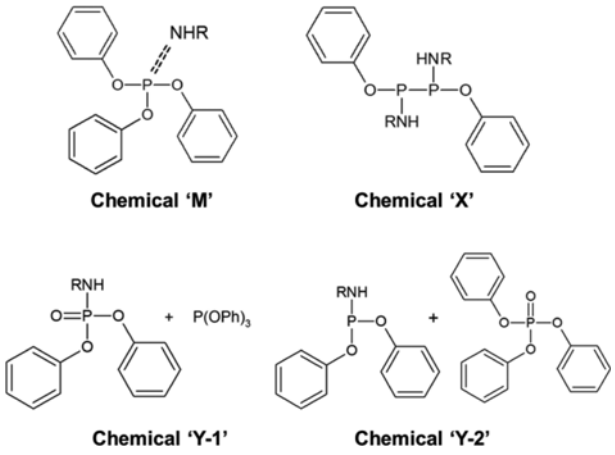

Scheme 1. Assigned chemicals from MS analysis.

N partial bond and consequent P-N intermediate species.

To further develop this assumption, we further used mass spectrometry (MS) with electrospray ionization (ESI) technique to identify two intermediates (Fig. 7). The analysis of these MS spectra suggests the presence of three observed species, denoted as chemical M, X, and Y, which can be assigned as 578 m/z, 781 m/z, and 809 m/z, respectively. Scheme 1 presents the molecular structure of expected chemicals M, X, and Y, which were chosen among the possible chemical species that can be produced by a series of reactions between TPP and OLA. Chemical M would be produced by reduction of TPP by OLA, forming partial P-N bond. Chemical X would be produced from P-O cleavage followed by dimerization from two M species, triggered by OLA and heating. We assigned chemical Y as chemical combination of Y-1 and Y-2, which can be altered from chemical M in the presence of ion beam energy during the MS measurement. Since ^{31}P NMR and DOSY analysis suggested two intermediates, which would be chemical M and X, chemical Y should be the chemical, obtainable only in the MS measurement process but not in the reaction between TPP and OLA. MS measurement is performed in ambient air, and therefore chemical M may be oxidized by incident high-energy ion beam during the measurement, to form phosphate-amine species as presented in the scheme of chemical Y-1. Then, the composite of TPP and phosphate-amine complex would be measured by MS, to exert MS signals of 809 m/z. In contrast, chemical Y-2 is less likely since it requires two simultaneous reactions of P-O bond cleavage of Chemical M and oxidation of TPP into triphenyl phosphate, followed by fusion of these two products to show 809 m/z signal.

CONCLUSION

This study suggests a novel synthetic approach of InP NCs using TPP. OLA readily activates TPP to become an effective P precursor. Control of temperature, reaction time, and the amount of $ZnCl_2$ enable one to produce various sizes of InP NCs, which absorption is in visible range. While InP cores do not show emission, adapting ZnS shell onto the NC surface makes the NCs luminescent, whose QY increases up to 23% (including 8% of band-edge emission). In addition, spectroscopic measurements provide a possible mechanism of TPP conversion that OLA forms partial bonds with TPP into amine-phosphite complexes. We believe that the proposed new approach of using novel P precursor will be an important milestone for designing not only InP NCs, but also other types of metal phosphides.

EXPERIMENTAL SECTION

1. Chemicals

Triphenyl phosphite (TPP, 97%), triethyl phosphite (TEP, 98%), indium(III) chloride ($InCl_3$, 98%), indium(III) acetate (99.99%), zinc(II) chloride ($ZnCl_2$, 99.999%), zinc stearate ($Zn(St)_2$, technical grade), zinc acetate ($Zn(Ac)_2$, 99.99%) 1-octadecene (ODE, 90%), oleylamine (OLA, 70%), oleic acid (OA, 90%), trioctylamine (TOA, 98%), sulfur (S, 99.998%), trioctylphosphine (TOP, 97%), and 1-dodecanethiol (DDT, 98%) were purchased from Sigma-Aldrich. Myristic acid (≥99%) was purchased from Tokyo Chemical Industry Co., Ltd. Tributylphosphine (TBP, ≥93%) was purchased from Wako. n-hexane (95.0%), acetone (99.5%), ethanol (99.5%), methanol (99.5%) and toluene (99.5%) were purchased from Samchum Chemicals. Benzene-D6 (D, 99.5%) and Chloroform D (D, 99.8%) were purchased from Cambridge Isotope Laboratories.

2. Characterization

TEM images were acquired using a Tecnai TF30 ST operated at 300 kV. TEM samples were prepared by drop-casting NC-hexane solution onto square mesh copper grids. The copper grids were dried under ambient air. UV-VIS spectra were obtained by a Shimadzu UV 3600 spectrometer. ICP-MS analysis was performed using an Agilent ICP-MS 7700S.

XRD analyses were performed using a RIGAKU Ultima IV at

40 kV and 40 mA with Cu K_α radiation (λ=1.5406 Å). X-ray diffraction samples were prepared by drop-casting NC-hexane solution onto Si substrates. Theta/2-theta mode was performed for sample measurement with sample pre-alignment for more reliable dataset.

For absolute PL quantum yield measurement, NC solution was diluted with toluene and transferred into a 1 cm quartz cuvette. Then, the cuvette was installed in a Hamamatsu Quantaurus-QY C11347 spectrometer equipped with an integrating sphere, calibrated with toluene as a reference.

For ^{1}H NMR, ^{31}P NMR, and DOSY, the sample flasks were transferred into Ar-filled glovebox after the reaction ceased, while keeping from air input. After being moved into glovebox, the 200 μm of the sample solution was mixed with 600 μm of bezene-d_6 or chloroform-d, then transferred to an NMR tube. The tube was sealed with Parafilm, and the measurements were performed using Agilent 400 MHz 54 mm NMR DD2 for ^{1}H and ^{31}P NMR, while DOSY spectra were recorded by Bruker Ultrastabilized^{TM} 900 MHz NMR spectrometer.

Electrospray Ionization (ESI) mass spectra were taken by Bruker Daltonik micrOTOF-Q II. Samples were further diluted with 100 equiv. volume of hexane before measurements. Mass spectra were recorded in positive charge detection mode.

3. Synthesis of InP NCs Using Phosphites

All reactants were opened and stored in Ar-filled glovebox, not to be exposed under the air. Solvents were degassed at 120 °C under vacuum for at least an hour, and stored in the glovebox. Typical InP NCs synthesis can be described as follows: $InCl_3$ (0.0444 g, 0.2 mmol), $ZnCl_2$ (0.1363 g, 1 mmol), OLA (1 ml, 3 mmol), and TOA (4.7 ml) were transferred into a 3-neck flask. When indium carboxylates were used as indium source, 0.2 mmol of indium carboxylate, 1 ml of OA, and 5 ml of ODE were mixed as reactant, instead of $InCl_3$, OLA, and ODE. The flask was connected to Schlenk line and was degassed further at 120 °C for 2 hours. The solution became transparent pale yellow color after the degassing process. After the degassing, the flask was filled with argon gas followed by heating to the desired reaction temperature (220 °C to 300 °C). At the desired temperature, the mixture of TPP (0.21 ml, 0.8 mmol) and TOA (0.5 ml) was rapidly injected. Aliquots were taken at the desired temperature using a glass syringe until the reaction was quenched. The resultant InP NCs were washed by centrifugation using methanol or ethanol as anti-solvent. The NCs were redispersed in hexane or toluene for measurements.

4. Growth of ZnS Shell on InP NCs

ZnS shell was formed on InP NCs using recipes modified from previously published methods [31,47-49]. The InP core was synthesized via the same procedure as previously described above.

For instance, ZnS shell was formed after the InP core formation in the same reaction flask without cooling after InP NC growth. 2.5 ml of 0.2 M $Zn(St)_2$ solution in TOA was injected. At the same time, 2 mmol of DDT (0.48 ml, degassed) was slowly injected over 2 min. The solution was heated to 300 °C and quenched after 1 hour. The resultant core/shell NCs were purified by centrifugation using ethanol.

ZnS shell would also be formed with other method of using zinc acetate and DDT in ODE. After the InP NCs were purified and redispersed in hexane solution, the InP-hexane solution was transferred to a reaction flask with 0.5 mmol of zinc acetate (0.0917 g) and 5 ml of ODE, followed by degassing process at 120 °C under vacuum. Afterwards, the reaction vessel was heated to 230 °C in Ar condition for 2 hour. Then, 0.2 mmol of DDT (48 μL) in 0.2 ml of ODE was injected. The reaction proceeded for 1 hour at 230 °C. Resultant NCs were purified by centrifugation using ethanol.

5. Synthesis of Phosphite-amine Intermediates for NMR, DOSY and MS

For NMR, DOSY and MS measurement, all samples were prepared in a 3-neck flask in Ar condition. All the chemicals were degassed before use. For the mixture of metal chloride, amine and phosphite, 0.2 mmol of $InCl_3$ (0.0444 g), 1 ml of OLA, 5.2 ml of TOA, and 1 ml of TPP were mixed and heated to 300 °C for an hour. For NMR, MS, and DOSY analysis of amine-phosphite mixtures, 0.5 ml of TPP, 5 ml of OLA, and 5 ml of TOA were mixed and heated at 230 °C for 1 hour. Some of chemicals would be excluded for a desired sample in these recipes. For instance, only 5 ml of OLA and 0.5 ml of TPP were mixed and heated to prepare the mixture of OLA and TPP.

ACKNOWLEDGEMENTS

This article was supported by the National Research Foundation (NRF) grant funded by the Korean Government (NRF-2016M3A7B4910618).

ABBREVIATIONS

InP	: indium phosphide
NC	: nanocrystal
LED	: light emitting diode
TOP	: trioctylphosphine
TPP	: triphenyl phosphite
$(TMS)_3P$	: tris(trimethylsilyl)phosphine
OLA	: oleylamine
TOA	: trioctylamine
DOSY	: diffusion ordered spectroscopy
MS	: mass spectroscopy
ESI	: electrospray ionization
DDT	: 1-dodecanethiol
ODE	: 1-octadecene

REFERENCES

1. A. P. Alivisatos, *J. Phys. Chem.*, **100**, 13226 (1996).
2. C. B. Murray, C. R. Kagan and M. G. Bawendi, *Annu. Rev. Mater. Res.*, **30**, 545 (2000).
3. D. V. Talapin and C. B. Murray, *Science*, **310**, 86 (2005).
4. W. D. Kim, D. Kim, D.-E. Yoon, H. Lee, J. Lim, W. K. Bae and D. C. Lee, *Chem. Mater.*, **31**, 3066 (2019).
5. Y. Shirasaki, G. J. Supran, M. G. Bawendi and V. Bulović, *Nat. Photonics*, **7**, 13 (2012).
6. J. Y. Woo, J.-H. Ko, J. H. Song, K. Kim, H. Choi, Y.-H. Kim, D. C. Lee and S. Jeong, *J. Am. Chem. Soc.*, **136**, 8883 (2014).
7. J. Y. Woo, S. Lee, S. Lee, W. D. Kim, K. Lee, K. Kim, H. J. An, D. C.

Lee and S. Jeong, *J. Am. Chem. Soc.*, **138**, 876 (2016).
8. J. Y. Woo, Y. Kim, J. Bae, T. G. Kim, J. W. Kim, D. C. Lee and S. Jeong, *Chem. Mater.*, **29**, 7088 (2017).
9. D. Kim, Y. K. Lee, D. Lee, W. D. Kim, W. K. Bae and D. C. Lee, *ACS Nano*, **11**, 12461 (2017).
10. X. Peng, L. Manna, W. Yang, J. Wickham, E. Scher, A. Kadavanich and A. P. Alivisatos, *Nature*, **404**, 59 (2000).
11. W. D. Kim, D.-E. Yoon, D. Kim, S. Koh, W. K. Bae, W.-S. Chae and D. C. Lee, *J. Phys. Chem. C*, **123**, 9445 (2019).
12. S. Koh, W. D. Kim, W. K. Bae, Y. K. Lee and D. C. Lee, *Chem. Mater.*, **31**, 1990 (2019).
13. J. Tersoff, C. Teichert and M. G. Lagally, *Phys. Rev. Lett.*, **76**, 1675 (1996).
14. B. G. Jeong, Y.-S. Park, J. H. Chang, I. Cho, J. K. Kim, H. Kim, K. Char, J. Cho, V. I. Klimov, P. Park, D. C. Lee and W. K. Bae, *ACS Nano*, **10**, 9297 (2016).
15. D. Kim, W. K. Bae, S.-H. Kim and D. C. Lee, *Nano Lett.*, **19**, 963 (2019).
16. W. D. Kim, W.-S. Chae, W. K. Bae and D. C. Lee, *Chem. Mater.*, **27**, 2797 (2015).
17. S. Hohng and T. Ha, *J. Am. Chem. Soc.*, **126**, 1324 (2004).
18. C. R. Kagan, C. B. Murray, M. Nirmal and M. G. Bawendi, *Phys. Rev. Lett.*, **76**, 1517 (1996).
19. M. Nirmal and L. Brus, *Acc. Chem. Res.*, **32**, 407 (1999).
20. C. Burda, X. Chen, R. Narayanan and M. A. El-Sayed, *Chem. Rev.*, **105**, 1025 (2005).
21. S. Koh and D. C. Lee, *MRS Commun.*, **8**, 742 (2018).
22. R. Xie, D. Battaglia and X. Peng, *J. Am. Chem. Soc.*, **129**, 15432 (2007).
23. O. I. Micic, C. J. Curtis, K. M. Jones, J. R. Sprague and A. J. Nozik, *J. Phys. Chem.*, **98**, 4966 (1994).
24. D. Battaglia and X. Peng, *Nano Lett.*, **2**, 1027 (2002).
25. A. A. Guzelian, J. E. B. Katari, A. V. Kadavanich, U. Banin, K. Hamad, E. Juban, A. P. Alivisatos, R. H. Wolters, C. C. Arnold and J. R. Heath, *J. Phys. Chem.*, **100**, 7212 (1996).
26. O. I. Micic, J. R. Sprague, C. J. Curtis, K. M. Jones, J. L. Machol, A. J. Nozik, H. Giessen, B. Fluegel, G. Mohs and N. Peyghambarian, *J. Phys. Chem.*, **99**, 7754 (1995).
27. J. Cui, A. P. Beyler, L. F. Marshall, O. Chen, D. K. Harris, D. D. Wanger, X. Brokmann and M. G. Bawendi, *Nat. Chem.*, **5**, 602 (2013).
28. S. Koh, T. Eom, W. D. Kim, K. Lee, D. Lee, Y. K. Lee, H. Kim, W. K. Bae and D. C. Lee, *Chem. Mater.*, **29**, 6346 (2017).
29. A. Singh, P. Chawla, S. Jain and S. N. Sharma, *Physica E*, **90**, 175 (2017).
30. L. Li, M. Protière and P. Reiss, *Chem. Mater.*, **20**, 2621 (2008).
31. E. Bang, Y. Choi, J. Cho, Y.-H. Suh, H. W. Ban, J. S. Son and J. Park, *Chem. Mater.*, **29**, 4236 (2017).
32. M. D. Tessier, D. Dupont, K. De Nolf, J. De Roo and Z. Hens, *Chem. Mater.*, **27**, 4893 (2015).
33. A. Buffard, S. Dreyfuss, B. Nadal, H. Heuclin, X. Xu, G. Patriarche, N. Mézailles and B. Dubertret, *Chem. Mater.*, **28**, 5925 (2016).
34. J. Liu, M. Meyns, T. Zhang, J. Arbiol, A. Cabot and A. Shavel, *Chem. Mater.*, **30**, 1799 (2018).
35. H. P. Andaraarachchi, M. J. Thompson, M. A. White, H.-J. Fan and J. Vela, *Chem. Mater.*, **27**, 8021 (2015).
36. J. R. Leto and M. F. Leto, *J. Am. Chem. Soc.*, **83**, 2944 (1961)
37. R. S. Vinal and L. T. Reynolds, *Inorg. Chem.*, **3**, 1062 (1964).
38. P. K. Khanna, K. W. Jun, K. B. Hong, J. Baeg and G. K. Mehrotra, *Mater. Chem. Phys.*, **92**, 54 (2005).
39. D. K. Harris and M. G. Bawendi, *J. Am. Chem. Soc.*, **134**, 20211 (2012).
40. A. J. Shin, J. J. Eun and J. E. Lim, Method for Preparing Metal Phosphide Nanocrystal From Phosphite Compound and Method for Passivating Nanocrystal Core with the Same, in: L. Samsung Electronics Co. (Ed.) Korea (2013).
41. H.-J. Byun, J. C. Lee and H. Yang, *J. Colloid Interface Sci.*, **355**, 35 (2011).
42. D. Caruntu, T. Rostamzadeh, T. Costanzo, S. S. Parizi and G. Caruntu, *Nanoscale*, **7**, 12955 (2015).
43. L. Hu, C. Wang, S. Lee, R. E. Winans, L. D. Marks and K. R. Poeppelmeier, *Chem. Mater.*, **25**, 378 (2013).
44. G. Laufersky, S. Bradley, E. Frécaut, M. Lein and T. Nann, *Nanoscale*, **10**, 8752 (2018).
45. K. Ando, M. Yamaguchi and C. Uemura, *Phys. Rev. B*, **34**, 3041 (1986).
46. H. P. Gislason and G. D. Watkins, *Phys. Rev. B*, **33**, 2957 (1986).
47. E. Ryu, S. Kim, E. Jang, S. Jun, H. Jang, B. Kim and S.-W. Kim, *Chem. Mater.*, **21**, 573 (2009).
48. A. Narayanaswamy, L. Feiner, A. Meijerink and P. Van der Zaag, *ACS Nano*, **3**, 2539 (2009).
49. W. Shen, H. Tang, X. Yang, Z. Cao, T. Cheng, X. Wang, Z. Tan, J. You and Z. Deng, *J. Mater. Chem. C*, **5**, 8243 (2017).
50. L. Li and P. Reiss, *J. Am. Chem. Soc.*, **130**, 11588 (2008).
51. S. Xu, J. Ziegler and T. Nann, *J. Mater. Chem.*, **18**, 2653 (2008).
52. J. Lim, W. K. Bae, D. Lee, M. K. Nam, J. Jung, C. Lee, K. Char and S. Lee, *Chem. Mater.*, **23**, 4459 (2011).
53. J. Lim, B. G. Jeong, M. Park, J. K. Kim, J. M. Pietryga, Y.-S. Park, V. I. Klimov, C. Lee, D. C. Lee and W. K. Bae, *Adv. Mater.*, **26**, 8034 (2014).